



# Fusion of Sentinel-1 and Sentinel-2 data in mapping the impervious surfaces at city scale

Binita Shrestha · Sajjad Ahmad ·  
Haroon Stephen

Received: 26 May 2021 / Accepted: 17 July 2021  
© The Author(s), under exclusive licence to Springer Nature Switzerland AG 2021

**Abstract** Urbanization creates new development in open spaces and agricultural fields, synonymous with increasing impervious surfaces. Such surfaces restrain the natural infiltration of water, and directly affect the non-point source pollution. Thus, consequential events like flooding and surface water degradation require spatial and quantitative information on impervious surfaces. Remote sensing technologies are widely used in impervious surface mapping of various geographical locations for environmental monitoring. In this study, the datasets from recently launched European Space Agency satellites (Sentinel-1 and Sentinel-2) and random forest classifier are used. The impervious surface growth of the study area, Lahore city, in 2015 and 2021, and growth trends are assessed. Results are validated with classification accuracy and comparison with similar datasets. The objective is to develop a reliable impervious surface mapping method with land cover quantification technique from multisource datasets. With a chi-square value of greater than 3.84 obtained from the McNemar test, the performance of fused data was superior to that of optical alone data in the classification. Over a 5-year period, Lahore grew at an annual rate of 2.14% comparable to the findings of Copernicus Land Services and the Atlas of Urban Expansion with an underestimation of 1% and 8.75%,

respectively. Improvements in overall accuracy (2.7%) and kappa coefficient (5%) were seen in classified maps from fused datasets. Fusion of Sentinel datasets provide a reliable means of impervious surface mapping at city scale as an indicator of environmental quality which is valuable for the sustainable management of the city.

**Keywords** Urban monitoring · Environmental monitoring · Land cover classification · Sentinel images · Data fusion · Random forest

## Introduction

Urban population is projected to exceed 70% of total in the middle of the twenty-first century (United Nations, 2008). Urbanization is a result of intricate socio-economic phenomena favoring economic growth, poverty reduction, and human development thereby making it inevitable (UN World Urbanization Prospects, 2018). Despite its global occurrence, the rate will differ among developed and developing nations (Birch & Wachter, 2011). Asia will be the main contributor of population surge by 2050. Ranagalage et al. (2021) shed light on the need to assess urban development and land use land cover (LULC) dynamics in Asian cities for urban planning. Besides the number, the size of urban areas is also growing. Angel et al. (2012) reported that 28 of the 30 cities under study expanded by more than 16-fold from 1900 to 2000, at twice the rate of their population growth.

B. Shrestha · S. Ahmad · H. Stephen (✉)  
Department of Civil and Environmental Engineering  
and Construction, University of Nevada Las Vegas,  
Las Vegas, NV 89154-4015, USA  
e-mail: haroon.stephen@unlv.edu

Accommodation of a growing population demands development by replacing natural landscape with concrete and asphalt surfaces. The concept of urbanization is thus interchangeable with the expansion of impervious surfaces (IS) of the cities. Expansion occurs at the cost of encroaching agricultural and natural land. Arnold and Gibbons (1996) consider IS as a principal indicator of the environmental and water budget impact of urbanization making environmental degradation as one of the pressing problems (Babaei et al., 2019; Venkatesan et al., 2011). IS prevent the percolation of water into the soil, disturbing the natural hydrology (Panahi et al., 2021). Barnes et al. (2001) also state that the asphalt and concrete act as “desert-like” hydrologically and generate large runoff volumes and discharge during intense storms. Consequences may include flash floods and relatively dry conditions shortly after, according to Christopherson (2001) (cited in Barnes et al., 2001). Dewan and Yamaguchi (2009), Adnan et al. (2020), and Roy et al. (2020) also connected the increase in flooding area with LULC dynamics. Concrete coverage hinders the natural system of absorbance and cleaning of stormwater due to declining forested land, agricultural land, wetlands, and other open spaces (Carter, 1961; Leopold, 1968).

Greater IS covers correspond to greater amounts of toxins, such as heavy metals and chemical pollutants, nutrients, pathogens, and sediments collected on the surfaces. These components are deposited in the receiving streams during rainfall events directly affects the non-point source (NPS) pollution (Arnold & Gibbons, 1996). Studies have also correlated the IS with the source contamination (Schueler, 1987) Even the underground sources are not spared (Klein, 1979) as recharge declines with increasing IS by reducing the base flow (Harbor & Jonathan, 1994; Pappas et al., 2008; Schueler et al., 2009; Rahaman et al., 2019). It is detrimental, as there is a large dependence on groundwater globally, with an annual withdrawal rate of 982 km<sup>3</sup> (Margat & vans der Gun, 2013). Increasing surface temperature is another result of IS expansion (Saher et al., 2021). With declining vegetation cover, less water is available for evapotranspiration, which diverts much solar energy into heat (Christopherson, 2001; Douglas, 1983; Saher et al., 2020). Heisler and Brazel (2010) confirm the difference in temperature between urban and surrounding rural surface due to urbanization process.

Alongside the change in LULC, densifying population and demands of urban environment result in exacerbation of air and water quality, high energy consumption, insufficient resources, challenged waste management, and urban flooding (National Geographic, n.d.; Thakali et al., 2018; Forsee & Ahmad, 2011; Bukhary et al., 2018). Therefore, sustainable environment management techniques are essential especially following the projected 2030 United Nations Sustainable Development Goals (SDGs) no. 6 (Clean Water and Sanitation) and 11 (Sustainable Cities and Communities) (United Nations, 2015). Land use modified for anthropogenic purposes also results in ecological destruction and habitat quality declination (Di Febbraro et al., 2018; Ibrahim Mahmoud et al., 2016; Kija et al., 2020) due to destruction and fragmentation of natural habitat patches (Watson et al., 2014) especially in developing countries due to overexploitation of natural resources for sustenance (Sweetman & Ezpeleta, 2017). Therefore, mapping the IS becomes essential for planned urban settlement and environmental monitoring.

Studies have sparked interest in the detection and analysis of impervious surfaces using remote sensing and studied its potential (Slonecker et al., 2001). Monday et al. (1994), Kienegger (1992), and Plunk et al. (1990) emphasize the knowledge on impervious surfaces in city planning efforts. RS images might be the only source of information for developing countries, though ground-based data and high-resolution imagery promise an accurate land cover and land use dataset (Fritz et al., 2017). But previous studies limit the LC dynamics assessment of South Asian cities with Landsat images. Subasinghe et al. (2016), Ranagalage et al. (2020), Naikoo et al. (2020), and Rizvi et al. (2020) are some of the examples of LULC studies in South Asian cities using medium-resolution Landsat images.

However, an alternative to medium resolution can be offered through high spatial and temporal resolution which is possible due to a mission of the sentinel family developed by the European Space Agency (ESA) (Phiri et al., 2020). Sentinel-1 (S-1) (A and B) is a pair of radar satellites launched in 2014 and 2016, respectively, while Sentinel-2 (S-2) (A and B) is a pair of optical satellites launched in 2015 and 2017, respectively. Attema et al. (2008) state that land surface mapping is one of the major applications of these satellites. With improved temporal, spectral, and spatial resolution, they are also compatible with other

optical and radar satellites such as Landsat, ERS-1, ERS-2, Envisat, and Radarsat (Davidson et al., 2010).

Phiri et al. (2020) emphasize the utilization of RS especially S-2 in enhancing global LULC monitoring. Although several studies have used S-1, S-2, or fusion of the images, Ranagalage et al. (2021) highlight that utilization of Sentinel data in South Asian cities is rare. The dataset fusion technique is burgeoning research in recent years, with a wide range of applications, including remote sensing (Blum & Liu, 2018). Fusion led to enhancement of spectral and spatial information from optical sensors by the sensitivity to dielectric properties and surface roughness of radar sensors (Mahyoub et al., 2019). Studies have used fusion to improve land use/land cover classification (Zhang et al., 2018; Sukawattanavijit & Chen, 2015; Waske & Benediktsson, 2007; McNairn et al., 2009; Hong et al., 2014; Stefanski et al., 2014). Studies also support the use of multi-sensor satellite data in classifying impervious surfaces in urban environments (Civco & Hurd, 1997; Ji & Jensen, 1999; Ridd, 1995). Despite their additive values, fusion of radar and optical sensors needs more exploitation (Joshi et al., 2016). There are three processing levels of fusion: pixel level, feature level, and decision level, the former being the most basic, which comprises geocoding and co-registration to stack the images' pixels (Pohl & Van Genderen, 1998). Alongside the ability to replace the medium resolution imagery such as Landsat, Sentinel data also lessens the economic burden of commercial imagery while enhancing the accuracy of classification. Together, radar and optical data can provide a wide range of reflectance and backscattering information from different land covers.

The remote sensing community recognizes random forest (RF) classifiers for their accuracy (Belgiu & Drăguț, 2016) with increasing application in land-cover classification (Chan & Paelinckx, 2008; Ghimire et al., 2010; Lawrence et al., 2006; Pal, 2005; Sesnie et al., 2008). Gislason et al. (2006) and Kulkarni and Lowe (2016) concluded the outperformance of RF when compared to other ensemble methods, maximum likelihood, minimum distance, decision trees, neural network, and support vector machine. Further, Rodriguez-Galiano et al. (2012) produced a land cover map for the province of Granada, Spain, with more than 90% accuracy using the algorithm.

Although fast-paced urbanization demands the need to track the impervious surface expansion in cities (Seto & Reenberg, 2014), developing countries lack a reliable source of information. Punjab Cities Growth Atlas (Sect. 3: Urban Expansion 50 Cities of Punjab) also uses Landsat data to conduct multitemporal urban assessment of 50 of the country's growing cities. Therefore, the current study utilizes combined S-1 and S-2 data to map the impervious surface of Lahore city with the RF algorithm.

Lahore was selected for the study as it represents one of the mega cities in the country and the capital of the most populous province, Punjab. Pakistan is no exception, with an annual urbanization rate at 3%, which is the fastest in South Asia (Kotkin & Cox, 2013). The whole of the city is considered as urbanized and also has a history of doubling its built-up surfaces within a decade from 1999 to 2011. This study aims to expand the available information on the city's growth rate and patterns of urbanization needed for sustainable development in the future.

In this research, the authors have mapped the impervious surface of Lahore city for the years 2015 and 2021. The objective is achieved by utilizing a remote sensing approach with data fusion of freely available Sentinel satellite imagery. The land cover classification to extract impervious surfaces is performed using random forest classifiers. The results were validated using unique pixels of each land cover from high-resolution images as well as from quantitative analysis with datasets from Angel et al. (2012) and Buchhorn et al. (2020). The classified maps from fused data were also compared with HRI scenes. The study also utilizes open-source software for image processing and classification. The radar-optical pairs have the potential to add values in terms of improved spatial resolution of (10 m), a wide range of spectrum from 442.7 to 2185.7 nm, backscattering information, and short revisit time (6 days) ("MultiSpectral Instrument Overview," n.d, para. 2). A cost-, time-, and labor-effective method is developed to update the impervious surface inventory, and examine the spatial growth pattern of the city, identifying the locations with impervious surface increases.

This paper is organized as follows. The study area and data are presented in "[Study area](#)" followed by methods in "[Methodology](#)." Then the results are given in "[Results](#)." Finally, discussion and conclusion

statements in “[Discussion](#)” and “[Conclusion](#)” terminate the paper.

## Study area

### Lahore city

The study area comprises Lahore city, which lies in the western most part of Pakistan, on the southern bank of the Ravi River as given in Fig. 1. The country is subdivided into five provinces. Its second largest province, Punjab, is the most populated with an urbanization rate of 36.71%; Lahore is its capital. The city, which was established 2000 years ago, is also the second largest in the country in terms of population. Its location is often defined as strategic, as it lies between two large and powerful countries, which has created disputes in the past. The city's

latitude and longitude coordinates are 31.582045, and 74.329376 (Fig. 1). It is the largest city in the province, with an area of 665 km<sup>2</sup> (as of 2015) and population of 11,126,285 (Pakistan Bureau of Statistics, [2017](#)). Among the 150 union councils (UCs) the city comprises, 122 are identified as urban and the remainder as rural/peri-urban (Punjab Bureau of Statistics, [2015](#)). Alongside being jeweled with historical monuments, the city is a famous education center and is flourishing in the tourism and entertainment sectors. The climate of the city is considered semi-arid (Köppen climate classification *BSh*), with May and January as the hottest and coldest months, respectively. Some past years faced extreme temperature fluctuations with a record high of 52.8 °C, and record low of –2.7 °C with snowfall in some parts, The Nation stated in their website as of November 6, 2016. The city receives an annual average rainfall of 628.88 mm (Wayback Machine,

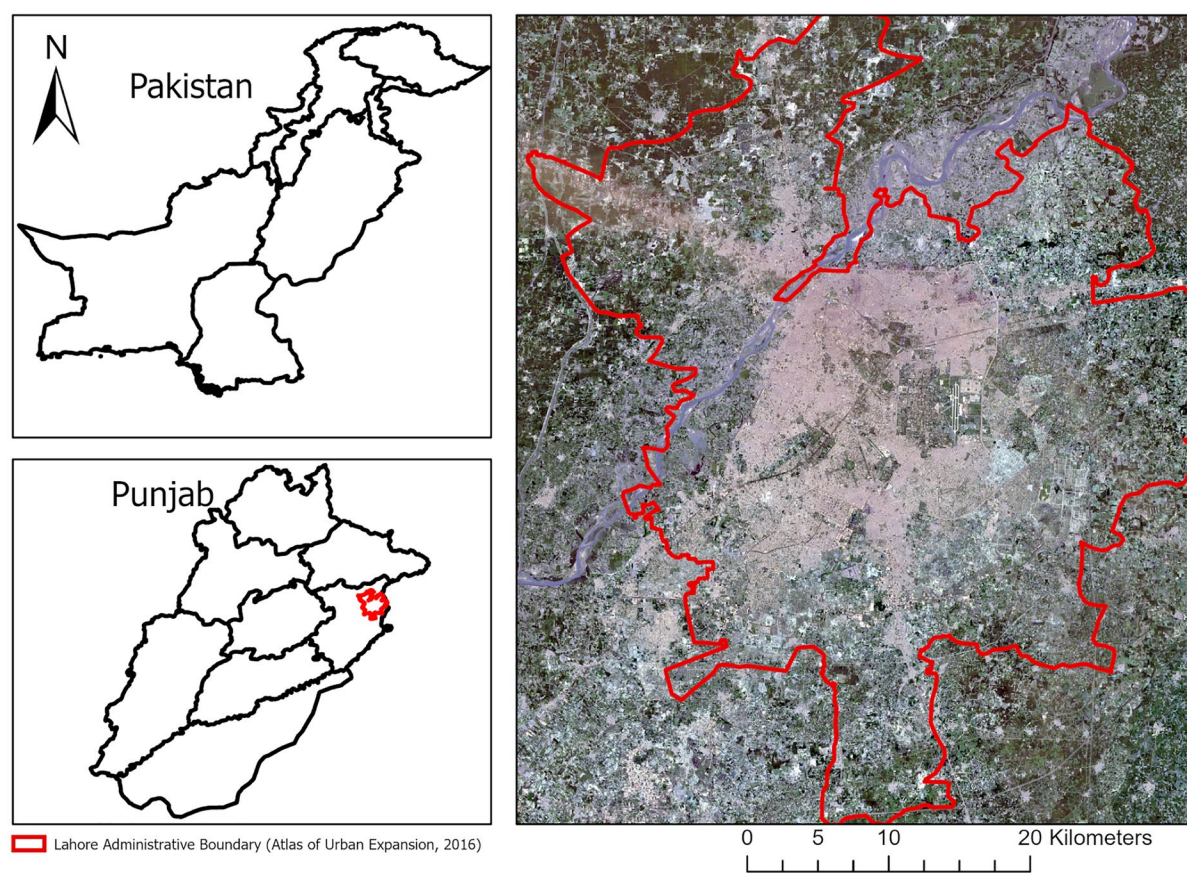


**Fig. 1** Map of the study area: Lahore city. True color composite from Sentinel 2 image (2015)

2010). Lahore has flat terrain with a mean sea level elevation of 217 m. Its eastern boundary holds the country's third busiest airport, Allama Iqbal International Airport ("History of Allama Iqbal International Airport, Lahore," 2016). Other features include the Upper Bari Doab Canal running through some parts of the city (Mujtaba et al., 2007). With just 3% green cover, impervious surfaces, or concrete cover, are prominent in the city.

## Dataset

This section explains the datasets used in this study to map the impervious surface of Lahore city and urban expansion analysis. The Sentinel family includes various sensors for land, ocean, and atmospheric monitoring. This study sheds light on S-1 and S-2 pairs. S-1 is an active radar satellite with a C-band Synthetic Aperture Radar (C-SAR) sensor. It operates at 5.405 GHz frequency. Among its various acquisition modes and product levels available for multiple uses, ground range detected (GRD) products in interferometric wide (IW) swath mode are apt for land monitoring. S-2 s, on the other hand, are passive satellites with Multispectral Instrument (MSI) optical sensors. They carry 13 spectral bands ranging from 0.443- to 2.190- $\mu\text{m}$  central wavelengths. Both sensors provide researchers with high-resolution images of up to 10-m spatial resolution and 6-day revisit

**Table 2** Acquisition dates of the images used in the study

Acquisition date	2015	Cloud cover (%)	2021	Cloud cover (%)
S-1 image	September 25	-	February 25	-
S-2 image	October 01	0	March 03	0.4

period. The specifications of the data used are listed in Table 1 below. Similarly, Table 2 has the date of image acquisition. 31.75° N and 74.58° E were used to define the extent of the city for image processing.

## Methodology

The following section describes the methodology used to achieve the objectives of the study. It is divided into five subsections: obtaining the images, preprocessing, classification, validation, and quantification. The detailed flowchart of the research methodology is illustrated in Fig. 2 and impervious area quantification in Fig. 3. The images of Lahore city were obtained from the Copernicus Open Access database for the years 2016 and 2020. SNAP and ArcGIS Pro were used to preprocess both S-1 and S-2 images and to prepare them for band stacking. RF classification algorithms were run in R software packages for land cover classification.

**Table 1** Sources and purpose of the datasets used in the study with specifications

Data	Purpose	Source	Spatial resolution	Temporal resolution	Sensor
S-1A	Classification and fusion	Copernicus Open Access Hub	10 m	6 days	SAR
S-2A	Classification and fusion	Copernicus Open Access Hub	10 m, 20 m, 60 m	5 days	MSI
DEM	Terrain correction	USGS	1 arc-sec	-	SRTM
High-resolution imagery	Pixel-based validation and comparative analysis	Google Earth Pro	15–15 cm	-	Combination of satellite images, aerial photos, and GIS data
Global land cover maps	Quantitative validation	Copernicus Land Service	100 m	1 year	Proba-V
Lahore land cover map	Quantitative validation	Angel et al. (2016)	30 m	-	OLI
Administrative boundary	Extent definition	Angel et al. (2016)	-	-	ESRI Shapefile

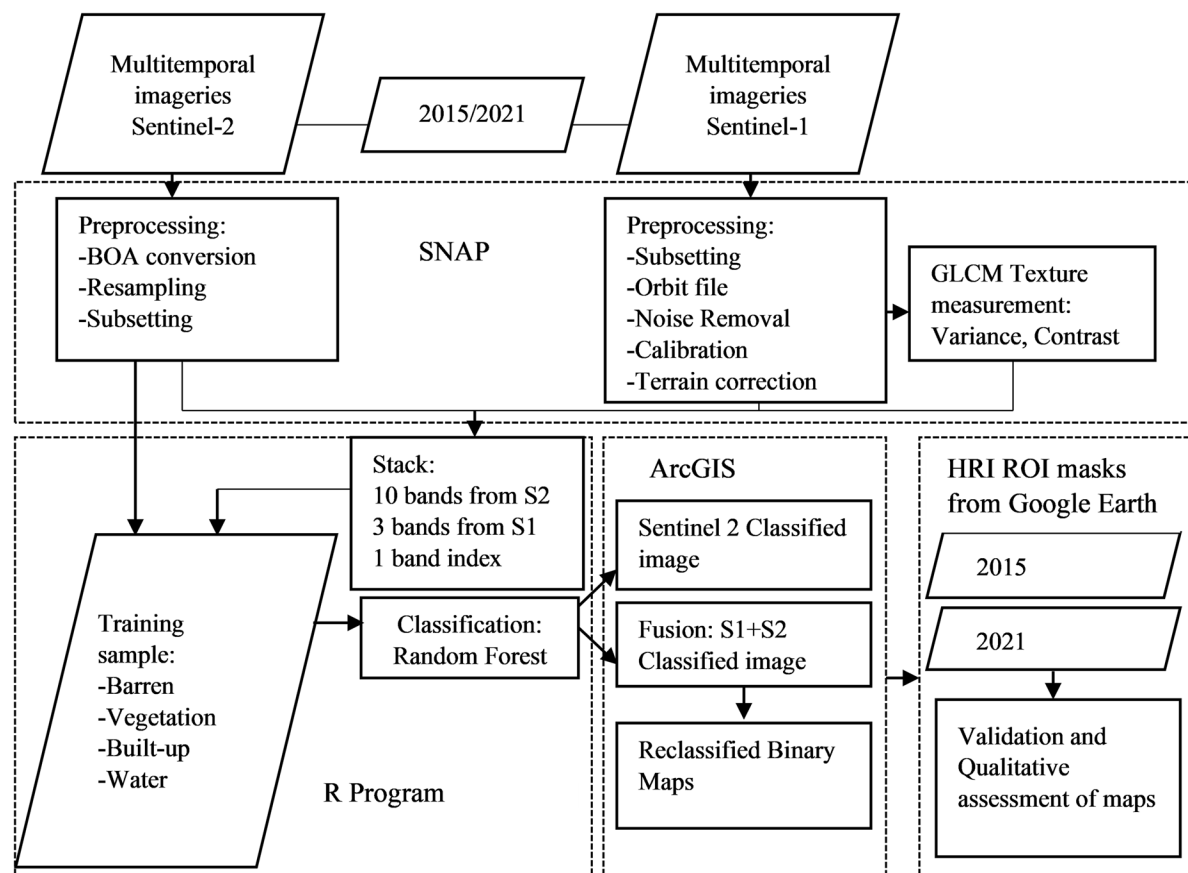


**Fig. 2** Overall framework of methodology to map the impervious surface of Lahore city

### Obtaining the images

This study uses S-1 and S-2 satellite images, accessed from the Copernicus Services Data Hub. The data hub provides an interactive interface to filter the date, satellite pairs, and cloud percentage for optical and acquisition mode for radar satellite images. Two images each from S-1 and S-2 for 2015 and 2021 for Lahore were obtained whose dates are given in Table 2. A region-of-interest box was created to define the extent of the city. The study time was chosen based on the largest time span covered by the satellites, along with the least cloud cover. While the cloud cover did not hinder the radar images, the optical mode, on the other hand, had frequent encounters. Therefore, S-2 limited the availability of images to some extent; as for fusion, the images were acquired from both sensors a few days apart.

### Preprocessing of the images

Preprocessing of the images was performed in two platforms: Sentinel Application Platform (SNAP) and ArcGIS Pro. The former is a collection of free open-source tool boxes developed by ESA. It supports the scientific exploitation of Earth observation missions: ERS-ENVISAT missions, Sentinels 1/2/3, Proba-V, and a range of National and third-party missions.

The first step of preprocessing the S-1 image was subsetting. We used the north, south, east, and west coordinates of the city of Lahore to crop the image into the extent of our interest. For consistency purposes we eliminated the VH polarization while subsetting the image from 2020 as the band was absent in the 2016 image. We then applied an updated orbit file to acquire accurate information on position and

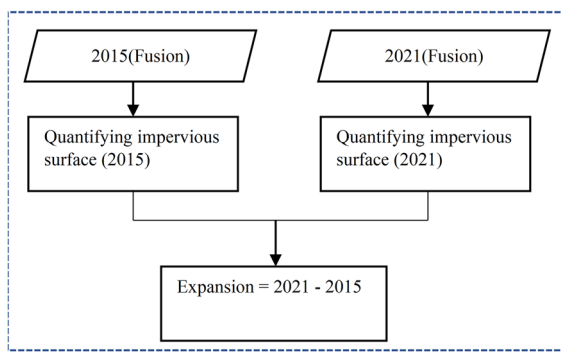


**Fig. 3** Quantification of impervious areas from 2015 to 2021

velocity of the satellite. SNAP allowed us to directly download the orbital information from the internet. Next, the low-intensity noise and invalid data on scene edges were removed by the border noise removal algorithm in SNAP (SNAP, 2019). Similarly, thermal noise removal algorithms were used to normalize the backscatter signal within the image scene. It was followed by calibration where the digital number of each pixel was converted into radiometrically calibrated SAR backscatter called sigma nought values. The information required for the calibration equation was contained in the metadata of the product in the form of look up tables (LUT). The backscatter values have a significant variation with properties of scattering surface (SNAP, 2019).

The side-looking geometry of the satellite creates some distortion in the image. Therefore, a range Doppler terrain correction algorithms was applied in SNAP for a more realistic geometric representation of the image. For such correction, reference digital elevation models were required for precise geolocation. One-arc-sec SRTM DEM data was used for the correction. The unit-less sigma nought values of the pixels were then converted to decibels using a logarithmic transformation (Filippone, 2019).

Finally, to gain additional information from the radar images, the computed texture measures were computed using the gray-level co-occurrence matrix (GLCM) in SNAP. The spatial relationships of pixels were captured by identifying the pattern based on the neighborhood size provided (Haralick, 1973; Jenicka & Suruliandi, 2014). The resultant matrix stores the occurrence frequency of pixel pairs with specific gray-level values ( $G$ ) (Haralick, 1973). Gray level indicates the brightness of a pixel. Depending

on the digitization depth, an image 12 bits deep has a minimum value of 0 and maximum of 4095 for  $G$ . A grayscale or color image can take any value within the range.  $G$  depends on both spatial orientation and displacement. Abdel-Hamid et al. (2018) state that such measures are common in image classification. However, Hall-Beyer (2017) argues that not all ten measures (offered in SNAP for GLCM computation) are apt for selection due to the existence of auto-correlation between some. Therefore, two of the four least correlated (Hall-Beyer, 2017) measures, contrast and variance (similar to Clerici et al., 2017), were chosen. A  $5 \times 5$  moving window for the neighborhood as well as single-pixel displacement was used (Clerici et al., 2017; Numbisi et al., 2018). Contrast measure provides the number of local variations in the image (Haralick et al., 1973) such as water bodies having comparatively lower values than grassland cover (Caballero et al., 2020). Similarly, variance emphasizes the partial characteristics of the radar image.

Though the S-1 image supports four cross polarizations (VV, VH, HV, and HH), radar images from 2020 had VV and VH channels, whereas the image from 2016 only had a VV channel. Therefore, for a consistent classification result, we eliminated the VH channel from the images of 2020 while subsetting, such that there were two additional bands in the form of texture measures in each radar image. Following the preprocessing, the S-1 images were re-projected to UTM zone 43 from WGS to align with the coordinate reference system (CRS) of S-2 images in ArcGIS.

Similarly, S-2 image preprocessing included atmospheric correction, resampling, and subsetting. For 2015, only top of atmosphere (TOA) level 1 products were accessible. Therefore, the sen2cor algorithm was applied in SNAP to convert the product into the bottom of atmosphere (BOA) level 2 product. This algorithm uses reflective properties of scene and cloud screening to establish accurate atmospheric and surface parameters. The series of corrections included cirrus correction, scene classification, aerosol optical thickness retrieval, and water vapor retrieval. Sen2cor correction eliminated band B10, as it only provides information on cirrus clouds, but not of the land (Main-Knorn et al., 2017). To stack the bands of S-1 and S-2, the spatial resolution, coordinate reference system (CRS), and extent of both images must match. However, S-2 products consist of multiple spatial resolutions within its 12 remaining bands. Thus, the next step was to resample

the product. The 20-m and 60-m S-2 bands were resampled in SNAP using a bilinear interpolation method. Finally, the north, south, east, and west coordinates of Lahore were used to crop the image into the extent of interest. Additionally, two bands, B1 and B9, which were originally 60 m in resolution, were removed while subsetting. The final product included 10 bands.

### Stacking

Stacking of bands from both sensors was performed in open-source software, R 4.2.0. In the final images, there were 14 features after stacking the images. Prior to stacking the bands, normalized built-up index (NDBI), a measure of build-up in urban surface (Zha et al., 2003), was developed using the following equation.

$$(NDBI) = \frac{SWIR(B11) - NIR(B8)}{SWIR(B11) + NIR(B8)} \quad (1)$$

where  $B11$  is a short-wave infrared band and  $B8$  is a near-infrared band. Built-up surfaces have relatively higher reflectance in band 11 (Kuc & Chormanski, 2019) than non built-up surfaces such as vegetation, water, and bare fields, which could be a useful feature for ISM. The S-1 image was then reprojected to the UTM (zone 43 N) coordinate system, and the extent of the image was adjusted to coincide that of the S-2 image, while preserving the resolution (10 m) prior to stacking the 10 bands from the S-2 image, 1 index, and 3 bands (VV polarization, variance, and contrast) from the S-1 image. Then using stack command in R, a RasterStack was formed that contained all 14 features combined in a single raster file. Such a stacking mechanism is also known as pixel-based fusion, which is the most preliminary level of multisensor image fusion.

### Random forest classification

RF works on the principle of growing diversified decision trees from different training data subsets through bagging. From the total features (14 in our case), a certain number of random features are selected to classify a new dataset. Each time, the dataset is classified by a specific number of trees (500 in our case, described later). From the training dataset provided, two-thirds

are randomly used to grow a decision tree, while the remaining become a part of another subset called out-of-bag (OOB). The process repeats for the training of the nth tree, where OOB elements can be classified each time for performance evaluation (Peters et al., 2007).

Number of trees [ntree( $k$ )] and number of features in each split [mtry ( $m$ )] are the significant components to determine the implementation of the RF classifier (Breiman, 2001). Thanh Noi and Kappas (2018) tested and evaluated the accuracy of the classifier by ranging the ntree as 100, 200, 500, and 1000, and mtry as 1:10 with a step size of 1. S-2 images with 10 bands were used for classification, equaling 10 variables for the classifier, and the same input dataset was for tuning all parameters. In their results, when mtry was equal to 2, 3, or 4, the overall accuracy with ntree equal to 200, 500, and 1000 did not differ much. Similarly, the OOB error plummeted when ntree increased from 1 to 100, while OOB error fell slightly in all datasets when ntree increased from 101 to 400. However, OOB error stabilized when ntree increased from 400 to 500, making it the optimal value. Therefore, in this study, 500 trees and 4 as the mtry value were employed throughout the land cover classification of Lahore. This method outputs the class that is the mode of the classes from individual trees (Ho, 1995, 1998). Accuracy is enhanced through utilizing individual tree strengths, while circumventing their weaknesses (Ghimire et al., 2010; Kotsiantis & Pin-telas, 2004).

Four RF models were trained, two for fused images with all 14 features, and another two for optical images with 11 features (deducting bands from radar image). Around 17,000 training pixels were extracted from the high-resolution image for different land covers to train the models. To comply with spatial arrangement of pixels in the satellite image, regular shapes for training polygons were created. Four land cover classes were defined for Lahore: built-up, barren, vegetation, and water. The built-up class included all the impervious surfaces such as roadways, runway, parking lots, pavements, and commercial and residential buildings. The samples were picked such that they were spread in all directions of the city. Each pixel was assigned a class by the RF model based on the best fit of reflectance value, NDBI value, backscattering value, and texture value with respect to the training set provided.

The classification was performed in R version 4.0.2 in a 64-bit processor. Both S-1 and S-2 images were imported as raster files with different bands as individual layers. For the S-2 image, a factor of 1/10,000 needs to be multiplied to the level-2A digital numbers (DN) of the pixels to gain surface reflectance values (Main-Knorn et al., 2017). Seventy-five percent of the training dataset was used to train the model, and rest to test the model. Since the objective is to assess how well the combination of bands from both satellite images can map the built-up surfaces, all of the 14 features were kept.

### Validation

The RF model uses a quarter of the training samples provided for the model testing purpose. The performance of the models was analyzed by the overall accuracy (OA) and kappa coefficient for the test set. The RF model first predicts the test set on its own and compares the result with the reference data. A confusion matrix is produced, and OA and kappa coefficients are computed from the matrix.

The RF models were used to predict the whole image of Lahore. The reliability of the resultant land cover maps was assessed using two measures, OA and kappa coefficient. For which a confusion matrix was prepared. The assessment was performed with all the four classes of land covers. It is to assure the quality and user confidence on the produced maps. Around 10,000 validation pixels were used which were unique to the training samples. Similar to training samples, validation pixels were also picked such that they cover all the directions in the city. The locations with heterogeneous land covers were chosen for robust accuracy assessment.

The land cover maps were reclassified into binary images with two classes, built-up and non-built-up, and performed a qualitative comparison with HRI with visual inspection. The corresponding scenes from the binary maps and HRI were arranged. Discussions on how well the maps were able to capture different land covers in those scenes were also made later in the result and discussion section. The binary maps were also quantitatively validated. For this, a comparative study of their results with two other published datasets was performed, which includes

Angel et al. (2016) and Buchhorn et al. (2020). The former studied a global sample of 200 cities with Lahore as one of them. As a result of the first two phases of their research, they produced extensive aspects of expansion of those cities. They have the urban extent data of Lahore for 2013 as well as rate of expansion from 2000 to 2013. The latter releases 100 m resolution annual land cover products from 2015 to 2019. The cover fractions present in the raw image were bare and sparse vegetation, built-up, cropland, forest, herbaceous vegetation, moss and lichen, seasonal inland water, shrubland, snow and ice, and permanent inland water (Buchhorn et al., 2020). A 20 × 20 degree tile which covers the whole area of Pakistan was downloaded for the intercomparison of the results.

### Quantification and spatial pattern analysis

The classified land cover maps were first reclassified into binary maps. The final maps contained built-up class and non-built-up class where vegetation, water, and barren classes were merged. The reclassified maps gave two values throughout the image extent, 1 denoting built-up and 0 denoting non-built-up classes. To quantify the impervious surface, the number of pixels identified as 1 was counted from the attribute table of the maps in ArcGIS and multiplied with the square of spatial resolution of the images i.e., 10 m. The values were then converted to square kilometers. The binary maps obtained from the fused dataset were then overlaid to observe the spatial pattern of growth in Lahore. Such practices are common among past studies (Aguejjad & Hubert-Moy, 2016; Hashidu et al., 2019).

## Results

This section provides the results from this study. Firstly, the final products of processed S-1 and S-2 images are presented. Then, the quantifications of Lahore's impervious surface area in 2015 and 2021 are presented, followed by the expansion rate acquired during the study period.

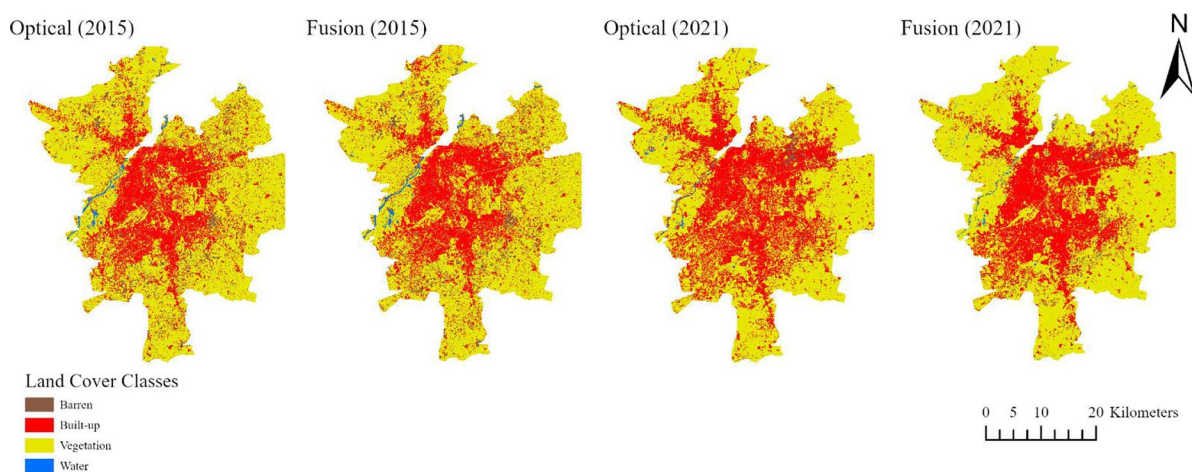


**Fig. 4** RF classification results of the Sentinel dataset (optical and fused) for 2015 and 2021

#### Processed and stacked images

The image preprocessing results include compatible radar and optical images for pixel-level fusion. There are two final radar images of Lahore for each year, 2015 and 2021. The first has only one band: sigma db. The second image has two bands: contrast texture and variance texture, while there is only one optical image of the city. Finally, a single product with 11 bands from the optical image and three bands from the radar image is obtained, which is later used for land cover map preparation.

#### Land cover maps

Figure 4 shows the RF land cover classification results of S-2 alone and the combined S-1 and S-2 dataset for 2015 and 2021, respectively. Four land covers are depicted by different colors: barren class as brown, built-up class as red, vegetation class as yellow, and water class as blue. Only a small area is covered by barren or open space, while vegetation cover

is significant. The vegetation cover includes tree cover, grassland, golf courses, and mostly cultivated land. The Ravi River flowing to the east of Lahore makes up most of the water class. The total area covered by each map is 1406.12 km<sup>2</sup>.

With RF, users have control over limited sources to improve the algorithm's performance, but the quality of land cover maps produced highly influences the accuracy of impervious surface mapping. Therefore, Abd Manaf et al. (2016) stated that training samples impact the quality of classification results. For instance, tuning the RF classifiers with varying numbers of trees and features to split the node does not affect the overall accuracy of the classification significantly, while the failure of missing some distinct land cover classes confuses the classifier when assigning a class to the pixel.

#### Results from validation

The validation results are presented in Tables 3 and 4 for the RF models and classified land cover maps,

**Table 3** Random forest model statistics for optical and fused images for 2016 and 2020

Model statistics							
2015				2021			
Optical		Fusion		Optical		Fusion	
OA (%)	Kappa	OA (%)	Kappa	OA (%)	Kappa	OA (%)	Kappa
98.2	0.97	99	0.98	97.5	0.96	98.7	0.98

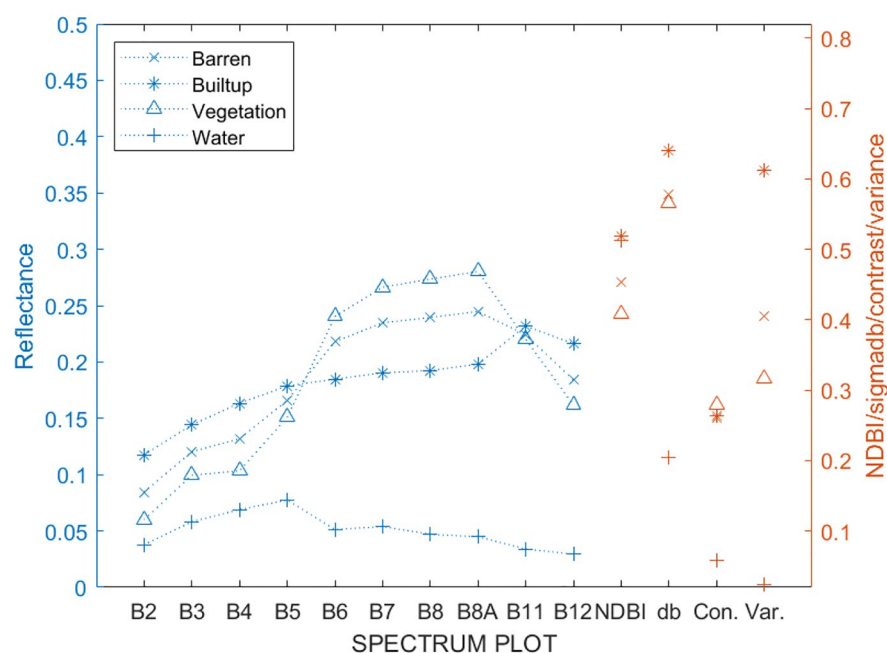
**Table 4** Overall accuracy and kappa coefficients of classified maps using optical and fused images

Validation result							
2015				2021			
Optical		Fusion		Optical		Fusion	
OA (%)	Kappa	OA (%)	Kappa	OA (%)	Kappa	OA (%)	Kappa
90.8	0.86	92.1	0.88	92.3	0.87	95	0.92

respectively. Table 3 shows that all the four models resulted in more than 95% overall accuracy, and more than a 0.95 kappa coefficient for the testing datasets. The model predicted 99% of the test data correctly for the fused dataset of 2015. From Table 4, the OAs of optical and fused data are 90.8% and 92.1%, respectively, and the kappa coefficients are 0.86 and 0.88, respectively, for 2015. This shows an improvement in the classification by 2%. Similarly, for 2021, the OAs of the optical and fused data are 92.3% and 95%, respectively, and the kappa coefficients are 0.87 and 0.92, respectively. This shows an improvement in the classification by 5%. Since the maps' OAs from all datasets are greater than 80%, 2%, or 5% improvement may not be significant to alter the quality and user confidence on the product. However, when city land cover maps are demanded during extreme weather or cloudy seasons, optical images alone may

not be suitable for map production. In such cases, improving the accuracy from 75 to 80% plays a significant role. An accuracy measure of greater than 80% is considered a good fit with the validation data. Therefore, radar images have the capacity to improve confidence in the produced land cover maps.

From the spectral signature plot in Fig. 5, some valuable information added by the radar bands in the land cover classification are identified. In the plot, it is seen that in the sigma db backscattering band and variance texture derived from radar image, built-up cover had the highest value, which could be important information for the RF classifiers. Such a distinct feature is helpful for the classifier in differentiating different land covers. This might have improved the overall accuracy and kappa coefficient of the classified maps from fused dataset. One optical image constraint is limited spectral resolution, which causes

**Fig. 5** Spectral signature of each land cover used in the classification for 2015 training data

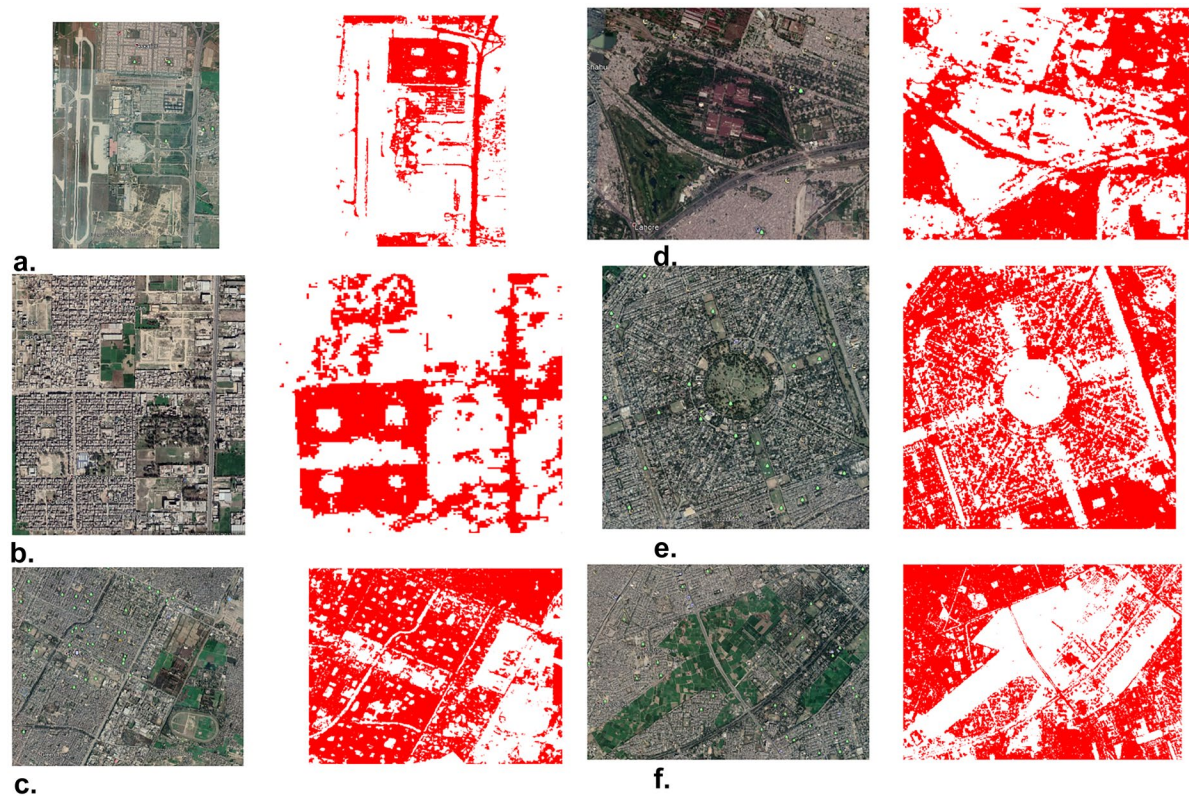


**Fig. 6** Comparison of classification with high-resolution image from Google Earth Pro (left column) for Lahore corresponding to 2021 classified fused image (right column)

different building roofs, roads, and parking lots to appear as different colors. This makes the automatic extraction of impervious surfaces challenging (Lu

et al., 2011). Therefore, Shaban and Dikshit (2001), Zhang et al. (2003), Puissant et al. (2005), Aguera et al. (2008), and Pacifici et al. (2009) suggest texture

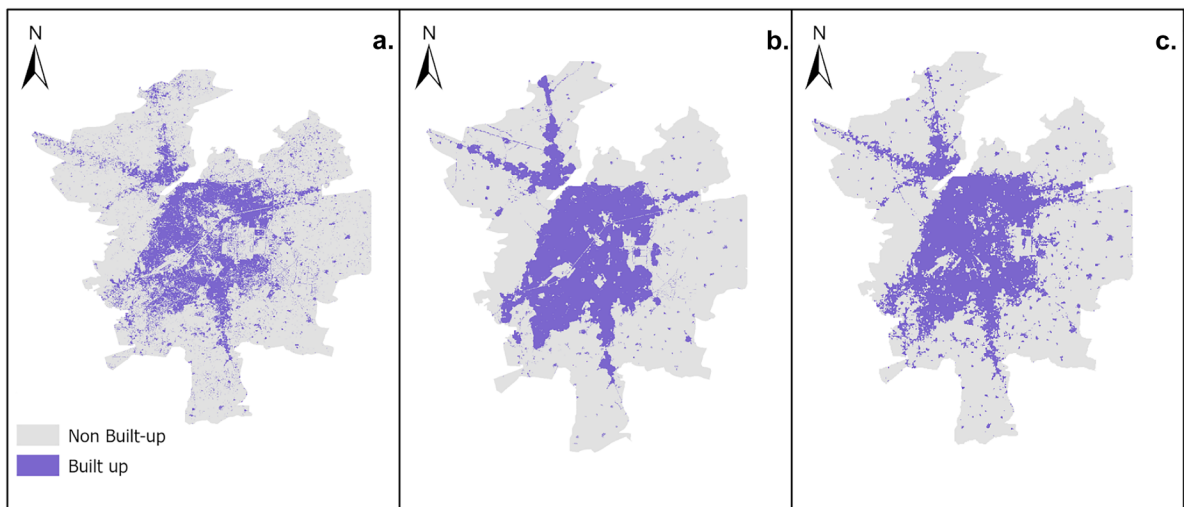


**Fig. 7** 2015 impervious surface mapping results from **a** this study, **b** Atlas of Urban Expansion, and **c** Copernicus Global Land Service

**Table 5** Comparison of impervious area computation with Angel et al. (2016) and Copernicus Global Land Service

2015 (CGLS) (km <sup>2</sup> )	2015 (Angel et al. (2012)) (km <sup>2</sup> )	2015 (fused image) (km <sup>2</sup> )
395.6 (+ 1%)	425 (+ 8.7%)	391.5

as one of the measures to reduce the impact of spectral variation within the same land cover (cited in Lu et al., 2011). Additionally, with free access to S-1 datasets, the calculation of texture measures is possible with low computational cost, unlike in the past.

Figure 6 illustrates the corresponding scenes from the binary maps and HRI side by side for a qualitative comparison of the impervious surface maps produced in this study. In Fig. 4a, the map partially captures the airport runway with distinct features of Lahore's ring road and the Askari X apartment complex to the North. Figure 3b, c show that agricultural fields, barren land, parks enclosed within housing settlements, and stadiums (Lahore race club) are not mixed with the built-up surface. Both densely populated settlements in Fig. 3d and buildings mixed with greenery in Fig. 3e are identified on the map. Additionally, in Fig. 3f, the built-up surface around the rich cultivated area is clearly differentiated. Through visual inspection, the impervious surface maps seem reliable in identifying the presence of dense, sparse, or fixed-shaped built-up surfaces in the city.

Figure 7 compares the binary maps from three different sources: current study, Angel et al. (2016), and Copernicus Global Land Service (CGLS). According to Angel et al. (2016), the urban extent of Lahore in 2013 was 396.3 km<sup>2</sup>. The study's urban extent included the following land covers: urban built-up, suburban built-up, rural built-up, urbanized open space, and exurban built-up areas. The authors computed a 3.6% average annual rate of urban extent expansion from 2000 to 2013 for the city. With this rate, Lahore's projected urban extent in 2015 was 425 km<sup>2</sup>. They utilized 30-m spatial resolution images from Landsat satellites. This area is 8.7% greater than the result produced in the current study.

**Table 6** Lahore's impervious surface area in 2021

Optical	488.9 km <sup>2</sup>
Fused	434.6 km <sup>2</sup>

Similarly, according to Buchhorn et al. (2020), the urban extent of Lahore in 2015 was 395.6 km<sup>2</sup>. They utilized 100-m spatial resolution images from Proba-V for their analysis. Their result is 1% greater than the result produced in the current study. The impervious surface areas of Lahore as computed from the above sources are given in Table 5.

### Result from quantification and spatial pattern analysis

In addition to improved classified map accuracy from fused data, it was also determined that the optical images overestimated the impervious area. Table 6 shows that the area of the city was 12.5% overestimated by the optical data. Therefore, further discussions are made using results obtained from fused images only.

The built-up and non-built-up cover of Lahore in 2015 and 2021 are given in Table 7. The results from Table 7 depict a clear urban expansion of Lahore in the past 5 years. In 2015, the city's impervious cover was 391.5 km<sup>2</sup>, and other land classes combined were 1014.62 km<sup>2</sup>. Impervious surfaces occupied 27.8% of the total study area. From Table 8, within 5 years, the city experienced a 43.1-km<sup>2</sup> increase in its impervious cover, increasing the share to 31%. The annual rate of expansion was found to be 2.14% from 2015 to 2021.

In Fig. 8, the impervious surface of Lahore in 2021 is denoted as red, and in 2015 it is denoted as purple for visual distinction. As depicted, the expansion took place on the edges of the settlement, as well as infilling in various places; however, edge expansion is dominant. Significant changes occurred in the southeastern and eastern directions. The five regions of interest (ROIs) delineated are referred to HRI for further analysis. Figure 9 illustrates the ROIs in 2015 and 2021 in the left and right columns, respectively. It is clear that the built-up surface area has surged either by extending from the established settlement, as in Fig. 9d, e; by densifying the settlement, as in Fig. 9 a, b; or by filling up the completely barren surface by new housing complexes, as in Fig. 9c.

The region in Fig. 9a is Paragon City. To accommodate Lahore's rising population, splendid but affordable housing is demanded. Therefore, the Paragon Company started development of the Paragon Housing Scheme Lahore in the region. As of 2020, December 23, Sky Marketing listed on its website

**Table 7** Lahore's impervious surface area from different datasets in 2015 and 2021

2015			2021			Annual urban expansion		
Built-up	Non-built-up	Cover	Built-up	Non-built-up	Cover			
391.5 km <sup>2</sup>	1014.62 km <sup>2</sup>	27.8%	434.6 km <sup>2</sup>	971.52 km <sup>2</sup>	31%			2.14%

that the region has easy access to several important city road networks, such as Barki Road, Ring Road, Jallo Road, Shabbir Sharif Road, and Zarrar Shaheed Road. The region in Fig. 9b is DHA phase 6. Housing societies, such as the Defense Housing Authority (DHA), have been expanding their projects in stages around Lahore. They are also expanding phase 7, while other phases ranging from 8 to 12 are under development. Likewise, the north of Qazi town in Fig. 9e, which was open agricultural land in late 2015, had been urbanized in the year 2021. This part of Lahore is known for its residential area, which is away from the hustle and bustle of the city, while Lahore Garden in Fig. 9d is known for its prime location. The housing scheme is located near the interchange of the Lahore-Islamabad Motorway, giving residents easy commuting to and from the rest of the city. The housing scheme is planning to add educational institutes and health care facilities that support the area's future growth (Lahore Garden Housing Scheme, n.d.). The expansion of residential and commercial places is accompanied by parking lots, pavements, roadways, and other built-up surfaces in those regions.

## Discussion

Previous studies mapping the impervious surface of Lahore using combined S-1 and S-2 data are not available; therefore, the result of the current study is compared with Angel et al.'s (2016) and Buchhorn et al.'s (2020) studies. The current study shows slight underestimation of impervious surface for the city (Table 5). The difference can be

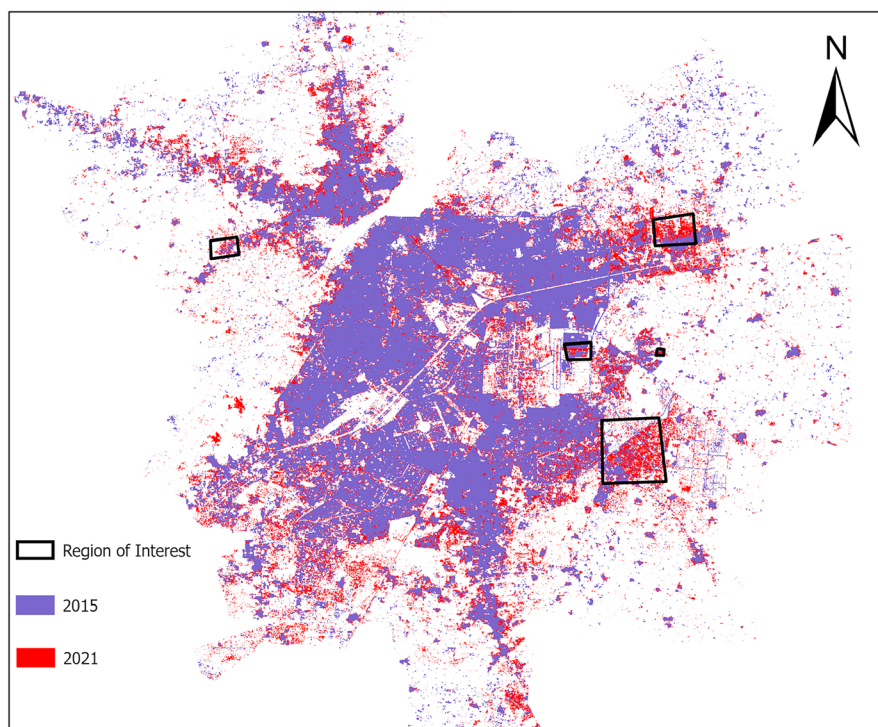
attributed to the spatial resolutions of the datasets used by the studies. From HRI in Google Earth, it was seen that in some distinct areas on the west and northwest of Lahore airport, built-up surfaces were heterogeneously mixed with grassland, trees, barren fields, and other open surfaces. In such areas, the land cover patches were lumped as built-up by the 30-m spatial resolution Landsat image and 100-m spatial resolution Proba-V images, while Sentinel was able to distinguish the land covers to some degree. Such differences indicate that certain regions of the city with heterogeneous covers, such as buildings with open spaces, grassland, and trees, can benefit more from high-resolution Sentinel images. Small and Lu (2006) also argued that urban mapping using Landsat TM/ETM+ data is challenging as urban areas comprise a mixture of manmade and vegetative land cover while only few pixels are pure urban.

There were instances where more accurate land cover land use (LCLU) classification was concluded from the fusion of multiple data (Zhang et al., 2018; Sukawattanavijit & Chen, 2015; Waske & Benediktsson, 2007; McNairn et al., 2009; Hong et al., 2014; Stefanski et al., 2014). Clerici et al. (2017) obtained overall accuracy of up to 88.75% with integration of texture from S-1 data and spectral information from S-2 data. Accuracy of classified land cover maps determines the efficiency of impervious cover mapping. More accurate information and more reliable environmental assessment can be conducted for the city. For example, the rate and pattern of IS expansion in Lahore are important for city planners to develop a warning system for urban flooding and proper allocation of resources. Rahman et al. (2021) concluded that land cover change, population growth, and road network growth had positive influence on the relative change in flooding area from Moran's *I* index. The conversion of agricultural land to built-up increased the flooding area whereas the vice versa had the opposite effect (Rahman et al., 2021) with

**Table 8** Analysis of impervious surface area expansion based on the total area of built-up surface from the classified maps

Study period	Change (km <sup>2</sup> )	Annual change (%)
2015–2021	43.1 km <sup>2</sup>	2.14

**Fig. 8** Spatio-temporal impervious surface expansion map of the study area (2015–2021) (based on the administrative boundary used in Angel et al. (2016))

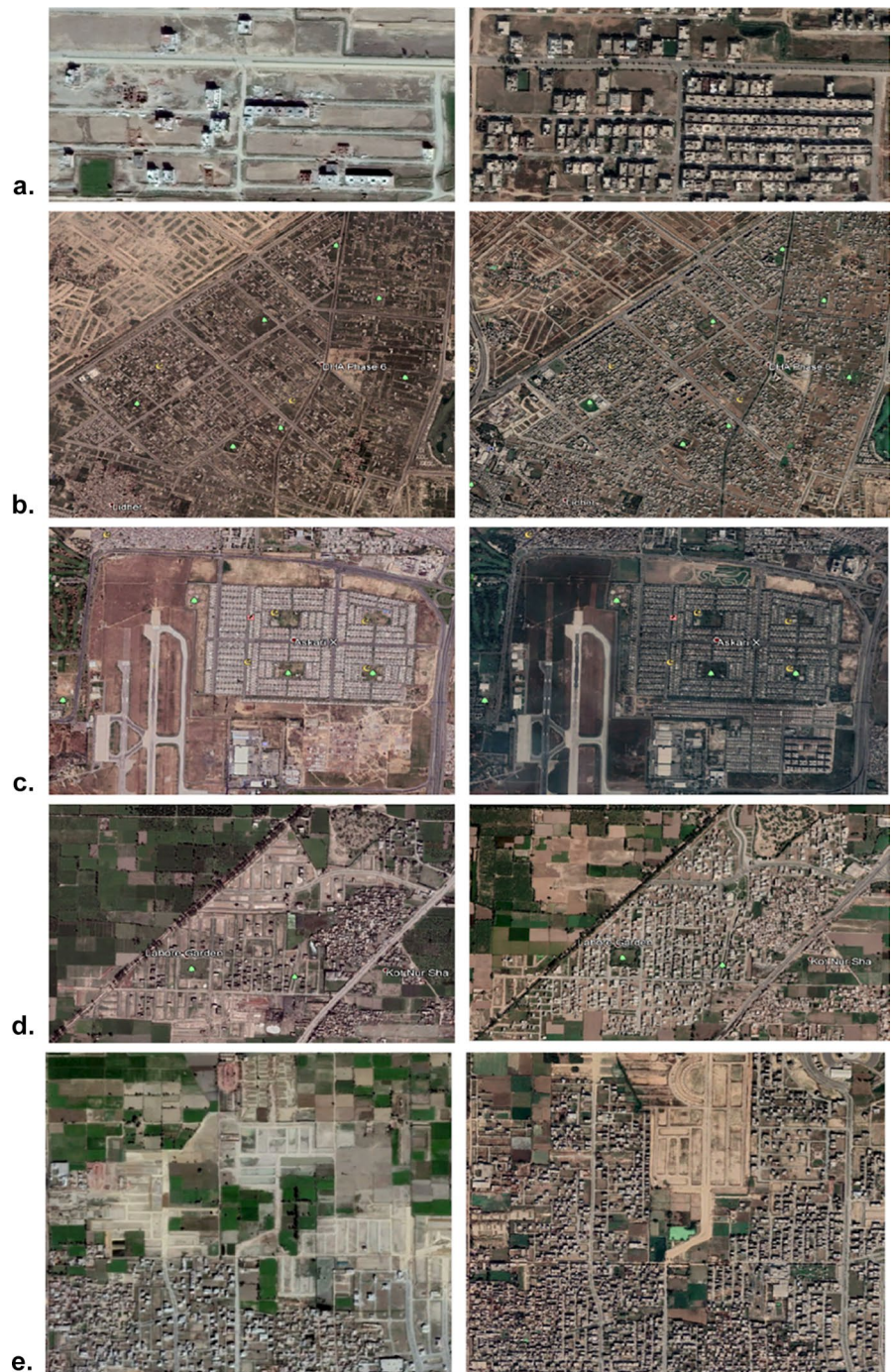


95% confidence interval in their regression model. A study by Zia and Shirazi (2019) concluded that every town of Lahore except Wahga was affected by urban flooding with increasing trends in the 2012–2017 monsoons. Every year, Lahore loses lives and properties due to ill-preparedness for the calamity. The stormwater drainage systems are encroached by expanding urban surfaces, which emphasizes the need to formulate policies to minimize the impact (Haider, 2018).

The method used in this research for change detection is known as a post-classification comparison technique (Alphan et al., 2009; Mas, 1999; Singh, 1989), which is considered a straightforward and intuitive change detection technique. According to Stow et al. (1980), the change maps are generally as accurate as the products of individual map accuracies, which makes the results from Fig. 6, 87% accurate (refer to Table 4 for map accuracies from 2015 and 2021). Wu et al. (2016) and Dewan and Yamaguchi (2009) used post-classification methods to detect and monitor land use/land cover change in Guangzhou city and Dhaka Metropolitan respectively.

Similarly, spatially identifying the built-up surfaces aid in listing the critical areas to emphasize on in sustainable future development (Ranagalage et al., 2021). They examined the LULC dynamics and urbanization pattern of four rapidly developing South Asian cities using S-2 data. The current study identified that Lahore is mostly developing in its East and Southeast directions. Ejiagha et al. (2020) chose the most accurate LULC map to derive land surface temperature (LST) map and quantified the inter-relationship of temperature with built-up surface again highlighting the importance of accuracy of land cover classification. Ejiagha et al. (2020) identified higher LST values in the residential and industrial areas with high density of impervious surface in Edmonton. The city in Canada had experienced a significant surge in population and dwellings in the past years (The City of Edmonton). Another study assessed the effect of LULC on LST in Mansehra and Battagram districts in Northern Pakistan also concluded that the built-up area had the highest value relative to bare soil, agriculture, and water (Ullah et al., 2019). Dewan et al. (2021) also confirmed imperviousness, lack of vegetation, and

**Fig. 9** Areas identified as impervious surface expansion in Lahore from 2015 (left column) to 2021 (right column) with visual inspection of overlaid maps from Google Earth Pro



population as major contributors to rise of urban temperature while determining factors controlling surface urban heat island intensity in five cities of Bangladesh. Thus results of the current study also help planners to mitigate urban heat island effect in the city

emphasizing activities such as plantation and decentralization of urban areas (Ullah et al., 2019).

There have been studies that focused on the environmental impacts of urban growth in Lahore city using RS, such as impervious area mapping with

operational land imager (OLI) imagery and Normalized Difference Built-up Index (NDBI) (Asad et al., 2017; Bhatti & Tripathi, 2014). Batool et al. (2019) concluded the expanding impervious surface due to conversion of agricultural land in the southeast of Lahore city was the principal cause behind the degrading groundwater source. Other studies have analyzed the relation between land surface temperature and land use change (Imran & Mehmood, 2020; Nasar-u-Minallah, 2020; Shah & Ghauri, 2015). In addition, this study contributes additional information on the expansion rate and pattern of Lahore from 2015 to 2021. Such information on impervious surfaces is an important indicator of environmental sustainability for the future development of the city.

## Conclusion

This research examined the pixel-level fusion of high spatial resolution data from S-1 and S-2 of Lahore to map the IS using RF classifiers. The rate of impervious surface expansion in the city in the last 5 years was computed with higher accuracy land cover maps obtained from combined radar and optical data. It was found that fused data improved the accuracy of the land cover maps by up to 5% in terms of OA and kappa coefficients, when compared to validation points from the very high-resolution images. Overall, among 10,000 samples, more than 90% were correctly predicted. The method developed in this study is cost, time, and labor effective. Optical data alone also produced similar accuracy, but the improvement added by the radar data can be valuable during extreme weather events. From the confusion matrix, it was clear that a greater number of built-up pixels were correctly identified by fused data. As in optical data, barren surfaces created spectral confusion, and the built-up surface was overestimated. The backscattering values from sigma db bands and variance texture measure provided additional distinct features to the classifier to improve the discrimination of built-up surfaces from barren surfaces. In the past 5 years, there has been a 43-km<sup>2</sup> increase in Lahore's IS, from 391.5 km<sup>2</sup> in 2015. The share of impervious areas increased from 27.8% to 31% in 5 years. The annual expansion rate was found to be 2.14%, and the expansion took place mainly on the city's edges. The major development was seen in the eastern and south-eastern directions. Some causes are development of

apartment complexes and housing space by DHA, as well as the construction of highways and ring roads.

**Author contribution** All authors have contributed equally to prepare this manuscript.

**Availability of data and materials** The data that support the findings of this study are available from the corresponding author upon reasonable request.

**Code availability** The codes used to generate the result of this study are available from the corresponding author upon reasonable request.

## Declarations

**Consent for publication** All the data used are open access and have been properly cited.

**Conflict of interest** The authors declare no competing interests.

## References

- Alphan, H., Doygun, H., & Unlukaplan, Y. I. (2009). Post-classification comparison of land cover using multi-temporal Landsat and ASTER imagery: the case of Kahramanmaraş, Turkey. *Environmental monitoring and assessment*, 151(1), 327–336.
- Abdel-Hamid, A., Dubovyk, O., El-Magd, A., & Menz, G. (2018). Mapping mangroves extend on the Red Sea coastline in Egypt using polarimetric SAR and high resolution optical remote sensing data. *Sustainability*, 10(3), 646.
- Abd Manaf, S., Mustapha, N., Sulaiman, M. N., Husin, N. A., & Hamid, M. R. A. (2016). Comparison of classification techniques on fused optical and SAR images for shoreline extraction: A case study at northeast coast of Peninsular Malaysia. *Journal of Computational Science*, 12(8), 399–411.
- Adnan, M. S. G., Abdullah, A. Y. M., Dewan, A., & Hall, J. W. (2020). The effects of changing land use and flood hazard on poverty in coastal Bangladesh. *Land Use Policy*, 99, 104868.
- Aguejjad, R., & Hubert-Moy, L. (2016). Monitoring urban growth using remote sensing and landscape metrics. Application to a medium-sized city, Rennes metropolitan area (France). *Cybergeo: European journal of geography*.
- Agüera, F., Aguilar, F. J., & Aguilar, M. A. (2008). Using texture analysis to improve per-pixel classification of very high-resolution images for mapping plastic greenhouses. *ISPRS Journal of Photogrammetry and Remote Sensing*, 63(6), 635–646.
- Angel, S., Blei, A. M., Civco, D. L., & Parent, J. (2012). *Atlas of urban expansion* (p. 397). Lincoln Institute of Land Policy.

- Angel, S., Blei, A. M., Civco, D. L., & Parent, J. (2016). *Atlas of urban expansion*. <http://atlasofurbanexpansion.org/cities/view/Lahore>
- Arnold, C. L., & Gibbons, C. J. (1996). Impervious surface coverage: The emergence of a key environmental indicator. *Journal of the American Planning Association*, 62(2), 243–258.
- Asad, M., Ahmad, S. R., Ali, F., Mehmood, R., Butt, M. A., & Rathore, S. Use of remote sensing for urban impervious surfaces: A case study of Lahore. *International Journal of Engineering and Applied Sciences*, 4(8), 257387.
- Attema, E., Davidson, M., Flory, N., Levriini, G., Rosich, B., Rommen, B., & Snoeij, P. (2008). Sentinel-1 ESA's new European radar observatory. In the 7th European conference on synthetic aperture radar (pp. 1–4). VDE.
- Babaei, H., Nazari-Sharabian, M., Karakouzian, M., & Ahmad, S. (2019). Identification of critical source areas (CSAs) and evaluation of best management practices (BMPs) in controlling eutrophication in the Dez River Basin. *Environments*, 6(2), 20.
- Barnes, K. B., Morgan, J., & Roberge, M. (2001). *Impervious surfaces and the quality of natural and built environments*. Department of Geography and Environmental Planning, Towson University.
- Batool, R., Mahmood, K., Ahmad, S. R., & Naeem, M. A. (2019). Geographic scenario of drinking water quality of Lahore metropolitan, Pakistan, in response to urbanization and water demand: A GIS perspective. *Applied Ecology and Environmental Research*, 17(2), 3973–3988.
- Belgiu, M., & Drăguț, L. (2016). Random forest in remote sensing: A review of applications and future directions. *ISPRS Journal of Photogrammetry and Remote Sensing*, 114, 24–31.
- Bhatti, S. S., & Tripathi, N. K. (2014). Built-up area extraction using Landsat 8 OLI imagery. *Giscience & Remote Sensing*, 51(4), 445–467.
- Birch, E. L., & Wachter, S. M. (Eds.). (2011). Global urbanization. University of Pennsylvania Press, 382p.
- Blum, R. S., & Liu, Z. (Eds.). (2018). Multi-sensor image fusion and its applications. CRC press.
- Breiman, L. (2001). Random Forests. *Machine Learning* 45, 5–32. <https://doi.org/10.1023/A:1010933404324>
- Buchhorn, M., Smets, B., Bertels, L., De Roo, B., Lesiv, M., Tsendbazar, N. E., Herold, M., & Fritz, S. (2020). *Copernicus global land service: land cover 100m; Collection 3: Epoch 2015: Globe 2020*. <https://doi.org/10.5281/zenodo.3939038>
- Bukhary, S., Batista, J., & Ahmad, S. (2018). Analyzing land and water requirements for solar deployment in the Southwestern United States. *Renewable and Sustainable Energy Reviews*, 82(3), 3288–3305. <https://doi.org/10.1016/j.rser.2017.10.016>
- Caballero, G. R., Platzeck, G., Pezzola, A., Casella, A., Winschel, C., Silva, S. S., Luduena, E., Pasqualotto, N., & Delegido, J. (2020). Assessment of multi-date sentinel-1 polarizations and GLCM texture features capacity for onion and sunflower classification in an irrigated valley: An object level approach. *Agronomy*, 10(6), 845.
- Carter, R. W. (1961). Magnitude and frequency of floods in suburban areas. Short Papers in the Geologic and Hydrologic Sciences, 424-B: B9–B11.
- Chan, J. C. W., & Paelinckx, D. (2008). Evaluation of random forest and Adaboost tree-based ensemble classification and spectral band selection for ecotope mapping using airborne hyperspectral imagery. *Remote Sensing of Environment*, 112(6), 2999–3011.
- Christopherson, R. W. (2001). *Elemental Geosystems* (3rd ed., p. 2001). Prentice Hall.
- Civco, D. L., & Hurd, J. D. (1997, April). Impervious surface mapping for the state of Connecticut. In *Proceedings of the 1997 ASPRS Annual Conference* (pp. 124–135).
- Clerici, N., Valbuena Calderón, C. A., & Posada, J. M. (2017). Fusion of Sentinel-1A and Sentinel-2A data for land cover mapping: A case study in the lower Magdalena region. *Colombia. Journal of Maps*, 13(2), 718–726.
- Davidson, M., Snoeij, P., Attema, E., Rommen, B., Flory, N., Levriini, G., & Duesmann, B. (2010, June). Sentinel-1 mission overview. In the 8th European Conference on Synthetic Aperture Radar (pp. 1–4). VDE.
- Dewan, A. M., & Yamaguchi, Y. (2009). Using remote sensing and GIS to detect and monitor land use and land cover change in Dhaka Metropolitan of Bangladesh during 1960–2005. *Environmental Monitoring and Assessment*, 150(1), 237–249.
- Dewan, A., Kiselev, G., Botje, D., Mahmud, G. I., Bhuiyan, M. H., & Hassan, Q. K. (2021). Surface urban heat island intensity in five major cities of Bangladesh: Patterns, drivers and trends. *Sustainable Cities and Society*, 71, 102926.
- Di Febbraro, M., Sallustio, L., Vizzarri, M., De Rosa, D., De Lisio, L., Loy, A., Eichelberger, B. A. & Marchetti, M. (2018). Expert-based and correlative models to map habitat quality: Which gives better support to conservation planning? *Global Ecology and Conservation*, 16, e00513.
- Douglas, I. (1983). *The Urban Environment*. Baltimore: Edward Arnold.
- Ejiagha, I. R., Ahmed, M. R., Hassan, Q. K., Dewan, A., Gupta, A., & Rangelova, E. (2020). Use of remote sensing in comprehending the influence of urban landscape's composition and configuration on land surface temperature at neighbourhood scale. *Remote Sensing*, 12(15), 2508.
- Forsee, W., & Ahmad, S. (2011). Evaluating urban stormwater infrastructure design in response to projected climate change. *ASCE Journal of Hydrologic Engineering*, 16(11), 865–873. [https://doi.org/10.1061/\(ASCE\)HE.1943-5584.0000383](https://doi.org/10.1061/(ASCE)HE.1943-5584.0000383)
- Filipponi, F. (2019). Sentinel-1 GRD preprocessing workflow. In *Multidisciplinary Digital Publishing Institute Proceedings* (Vol. 18, No. 1, p. 11).
- Fritz, S., See, L., Perger, C., McCallum, I., Schill, C., Schepaschenko, D., Duerauer, M., Karner, M., Dresel, C., Laso-Bayas, J., Lesiv, M., Moorthy, I., Salk, C.F., Danylo, O., Sturm, Albrecht, F., You, L., Kraxner, F., & Obersteiner, M. (2017). A global dataset of crowdsourced land cover and land use reference data. *Scientific data*, 4, 170075.
- Ghimire, B., Rogan, J., & Miller, J. (2010). Contextual land-cover classification: Incorporating spatial dependence in land-cover classification models using random forests and the Getis statistic. *Remote Sensing Letters*, 1(1), 45–54.
- Gislason, P. O., Benediktsson, J. A., & Sveinsson, J. R. (2006). Random forests for land cover classification. *Pattern Recognition Letters*, 27(4), 294–300.
- Haider, Z. (2018). Lessons from Lahore flooding. *International The News, Money Matters*.

- Hall-Beyer, M. (2017). Practical guidelines for choosing GLCM textures to use in landscape classification tasks over a range of moderate spatial scales. *International Journal of Remote Sensing* 38(5), 1312–1338.
- Haralick, R. M., Shanmugam, K., & Dinstein, I. H. (1973). Textural features for image classification. *IEEE Transactions on Systems, Man, and Cybernetics*, 6, 610–621.
- Harbor, & Jonathan M. (1994). A practical method for estimating the impact of land-use change on surface runoff, groundwater recharge and wetland hydrology. American Planning Association. *Journal of the American Planning Association* 60 (1).
- Hashidu, B. R., Abbas, A. M., & Kamaludeen, A. M. (2019). Urban growth pattern and agricultural land use dynamics in Gombe City, Nigeria. *Journal of Advanced Research in Agriculture Science and Technology*, 2(2), 43–49.
- Heisler, G. M., & Brazel, A. J. (2010). The urban physical environment: temperature and urban heat islands. Chapter 2. In: Aitkenhead-Peterson, Jacqueline; Volder, Astrid, eds. *Urban Ecosystem Ecology*. Agronomy Monograph 55. Madison, WI: American Society of Agronomy, Crop Science Society of America, Soil Science Society of America: 29–56, 29–56.
- History of Allama Iqbal International Airport, Lahore. (2016, June 9). CAA. <http://lahoreairport.com.pk/About/About-History.aspx/>
- Ho, T. K. (1995). Random decision forests. In *Proceedings of 3rd international conference on document analysis and recognition* (Vol. 1, pp. 278–282). IEEE.
- Ho, T. K. (1998). The random subspace method for constructing decision forests. *IEEE Transactions on Pattern Analysis and Machine Intelligence*, 20(8), 832–844.
- Hong, G., Zhang, A., Zhou, F., & Brisco, B. (2014). Integration of optical and synthetic aperture radar (SAR) images to differentiate grassland and alfalfa in Prairie area. *International Journal of Applied Earth Observation and Geoinformation*, 28, 12–19.
- Ibrahim Mahmoud, M., Duker, A., Conrad, C., Thiel, M., & Shaba Ahmad, H. (2016). Analysis of settlement expansion and urban growth modelling using geoinformation for assessing potential impacts of urbanization on climate in Abuja City. *Nigeria. Remote Sensing*, 8(3), 220.
- Imran, M., & Mehmood, A. (2020). Analysis and mapping of present and future drivers of local urban climate using remote sensing: A case of Lahore. *Pakistan. Arabian Journal of Geosciences*, 13(6), 1–14.
- Jenicka, S., & Suruliandi, A. (2014). A textural approach for land cover classification of remotely sensed images. *CSIT*, 2, 1–9. <https://doi.org/10.1007/s40012-014-0038-4>
- Ji, M., & Jensen, J. R. (1999). Effectiveness of subpixel analysis in detecting and quantifying urban imperviousness from Landsat Thematic Mapper imagery. *Geocarto International*, 14(4), 33–41.
- Joshi, N., Baumann, M., Ehammer, A., Fensholt, R., Grogan, K., Hostert, P., & Waske, B. (2016). A review of the application of optical and radar remote sensing data fusion to land use mapping and monitoring. *Remote Sensing*, 8(1), 70.
- Kienegger, E. H. (1992). Assessment of a wastewater service charge by integrating aerial photography and GIS. *Photogrammetric Engineering and Remote Sensing*, 58(11), 1601–1606.
- Kija, H. K., Ogutu, J. O., Mangewa, L. J., Bukombe, J., Verones, F., Graae, B. J., Kidegheso, J. R., Said, M. Y., & Nzunda, E. F. (2020). Spatio-temporal changes in wildlife habitat quality in the greater Serengeti ecosystem. *Sustainability*, 12(6), 2440.
- Klein, R. (1979) Urbanization and stream quality impairment. American Water Resources Association, Water Resources Bulletin, 15(4).
- Kotkin, J., & Cox, W. (2013, April 8) The world's fastest-growing megacities. *Forbes*.
- Kotsiantis, S., & Pintelas, P. (2004). Combining bagging and boosting. *International Journal of Computational Intelligence*, 1(4), 324–333.
- Kuc, G., & Chormański, J. (2019). Sentinel-2 imagery for mapping and monitoring imperviousness in urban areas. *International Archives of the Photogrammetry, Remote Sensing and Spatial Information Sciences*, 42(1/W2).
- Kulkarni, A. D., & Lowe, B. (2016). Random forest algorithm for land cover classification.
- Lahore Garden Housing Scheme. (n.d.). Zameen. [https://www.zameen.com/new-projects/lahore\\_garden\\_housing\\_scheme-442.html#overview](https://www.zameen.com/new-projects/lahore_garden_housing_scheme-442.html#overview). (accessed on 6 April 2021).
- Lawrence, R. L., Wood, S. D., & Sheley, R. L. (2006). Mapping invasive plants using hyperspectral imagery and Breiman Cutler classifications (RandomForest). *Remote Sensing of Environment*, 100(3), 356–362.
- Leopold, L. B. (1968). Hydrology for urban land planning: A guidebook on the hydrologic effects of urban land use (Vol. 554). US Geolgoical Survey. 1968, 554.
- Lu, D., Hetrick, S., & Moran, E. (2011). Impervious surface mapping with Quickbird imagery. *International Journal of Remote Sensing*, 32(9), 2519–2533.
- Mahyoub, S., Fadilb, A., Mansour, E. M., Rhinanea, H., & Al-Nahmia, F. (2019). Fusing of optical and synthetic aperture radar (SAR) remote sensing data: A systematic literature review (SLR). *International Archives of the Photogrammetry, Remote Sensing and Spatial Information Sciences*, 42(4/W12).
- Main-Knorn, M., Pflug, B., Louis, J., Debaecker, V., Müller-Wilm, U., & Gascon, F. (2017). Sen2Cor for sentinel-2. In *Image and Signal Processing for Remote Sensing XXIII* (Vol. 10427, p. 1042704). International Society for Optics and Photonics.
- Margat, J., & van der Gun, J. (2013). *Groundwater around the world: A geographic synopsis*. CRC Press/Balkema.
- Mas, J. F. (1999). Monitoring land-cover changes: a comparison of change detection techniques. *International journal of remote sensing*, 20(1), 139–152.
- McNairn, H., Champagne, C., Shang, J., Holmstrom, D., & Reichert, G. (2009). Integration of optical and Synthetic Aperture Radar (SAR) imagery for delivering operational annual crop inventories. *ISPRS Journal of Photogrammetry and Remote Sensing*, 64(5), 434–449.
- Monday, H. M., Urban, J. S., Mulawa, D., & Benkelman, C. A. (1994). City of Irving utilizes high resolution multispectral imagery for NPDES compliance. *Photogrammetric Engineering and Remote Sensing*, 60(4), 411–416.

- Mujtaba, G., Ahmed, Z., & Ophori, D. (2007). Management of groundwater resources in Punjab, Pakistan, using a groundwater flow model. *Journal of Environmental Hydrology*, 15, 1–14.
- MultiSpectral Instrument (MSI) Overview. (n.d.). ESA Sentinel Online. <https://dragon3.esa.int/web/sentinel/technical-guides/sentinel-2-msi/msiinstrument>. (accessed on February 1, 2021).
- Nasar-u-Minallah, M. (2020). Exploring the relationship between land surface temperature and land use change in Lahore using Landsat data. *Pakistan Journal of Scientific & Industrial Research Series A: Physical Sciences*, 63(3), 188–200.
- National Geographic. Urbanization causes and impacts. Urban Threats. Available online: <https://www.nationalgeographic.com/environment/habitats/urban-threats/>. (accessed on 6 July 2021).
- Naikoo, M. W., Rihan, M., & Ishtiaque, M. (2020). Analyses of land use land cover (LULC) change and built-up expansion in the suburb of a metropolitan city: Spatio-temporal analysis of Delhi NCR using landsat datasets. *Journal of Urban Management*, 9(3), 347–359.
- Numbisi, F. N., Van Coillie, F., & De Wulf, R. (2018). Multi-date Sentinel 1 SAR image textures discriminate perennial agroforests in a tropical forest-savanna transition landscape. *International Archives of the Photogrammetry, Remote Sensing & Spatial Information Sciences*, 42(1).
- Pacifici, F., Chini, M., & Emery, W. J. (2009). A neural network approach using multi-scale textural metrics from very high-resolution panchromatic imagery for urban land-use classification. *Remote Sensing of Environment*, 113(6), 1276–1292.
- Pakistan Bureau of Statistics. (2017). District and tehsil level population summary with region breakup. Retrieved from <http://www.pbscensus.gov.pk>
- Pal, M. (2005). Random forest classifier for remote sensing classification. *International Journal of Remote Sensing*, 26(1), 217–222.
- Panahi, M., Khosravi, K., Ahmad, S., Panahi, S., Heddam, S., Melesse, A. M., Omidvar, E., & Lee, C.-W. (2021). Cumulative infiltration and infiltration rate prediction using optimized deep learning algorithms: A study in Western Iran. *Journal of Hydrology: Regional Studies*, 35, 100825. <https://doi.org/10.1016/j.ejrh.2021.100825>
- Pappas, E. A., Smith, D. R., Huang, C., Shuster, W. D., & Bonta, J. V. (2008). Impervious surface impacts to runoff and sediment discharge under laboratory rainfall simulation. *CATENA*, 72(1), 146–152.
- Peters, J., De Baets, B., Verhoest, N. E., Samson, R., Degroeve, S., De Becker, P., & Huybrechts, W. (2007). Random forests as a tool for ecohydrological distribution modeling. *ecological modelling*, 207(2–4), 304–318.
- Phiri, D., Simwanda, M., Salekin, S., Nyirenda, V. R., Murayama, Y., & Ranagalage, M. (2020). Sentinel-2 data for land cover/use mapping: A review. *Remote Sensing*, 12(14), 2291.
- Plunk, D. E., Morgan, K., & Newland, L. (1990). Mapping impervious cover using Landsat TM data. *Journal of Soil and Water Conservation*, 45(5), 589–591.
- Pohl, C., & Van Genderen, J. L. (1998). Review article multisensor image fusion in remote sensing: Concepts, methods and applications. *International Journal of Remote Sensing*, 19(5), 823–854.
- Puissant, A., Hirsch, J., & Weber, C. (2005). The utility of texture analysis to improve per-pixel classification for high to very high spatial resolution imagery. *International Journal of Remote Sensing*, 26(4), 733–745.
- Punjab Bureau of Statistics. (2015). Punjab development statistics 2015. Lahore (2015). Retrieved from <http://www.bos.gov.pk/publicationreports>
- Rahaman, M. M., Thakur, B., Kalra, A., & Ahmad, S. (2019). Modeling of GRACE-derived groundwater information in the Colorado River Basin. *Hydrology*, 6(1), 19.
- Rahman, M., Ningsheng, C., Mahmud, G. I., Islam, M. M., Pourghasemi, H. R., Ahmad, H., Habumugisha, J. M., Washashg, R. M. A., Alam, M., Liu, E., Han, Z., Ni, H., Shufeng, T., & Dewan, A. (2021). Flooding and its relationship with land cover change, population growth, and road density. *Geoscience Frontiers*, 12(6), 101224.
- Ranagalage, M., Ratnayake, S. S., Dissanayake, D. M. S. L. B., Kumar, L., Wickremasinghe, H., Vidanagama, J., Cho, H., Udagedara, S., Jha, K. K., Simwanda, M., Phiri, D., Perera, E., & Muthunayake, P. (2020). Spatiotemporal variation of urban heat islands for implementing nature-based solutions: A case study of Kurunegala, Sri Lanka. *ISPRS International Journal of Geo-Information*, 9(7), 461.
- Ranagalage, M., Morimoto, T., Simwanda, M., & Murayama, Y. (2021). Spatial analysis of urbanization patterns in four rapidly growing South Asian cities using Sentinel-2 data. *Remote Sensing*, 13(8), 1531.
- Ridd, M. K. (1995). Exploring a V-I-S (vegetation-impermeous surface-soil) model for urban ecosystem analysis through remote sensing: Comparative anatomy for cities. *International Journal of Remote Sensing*, 16(12), 2165–2185.
- Rizvi, S. H., Fatima, H., Iqbal, M. J., & Alam, K. (2020). The effect of urbanization on the intensification of SUHIs: Analysis by LULC on Karachi. *Journal of Atmospheric and Solar-Terrestrial Physics*, 207, 105374.
- Rodriguez-Galiano, V. F., Ghimire, B., Rogan, J., Chica-Olmo, M., & Rigol-Sánchez, J. P. (2012). An assessment of the effectiveness of a random forest classifier for land-cover classification. *ISPRS Journal of Photogrammetry and Remote Sensing*, 67, 93–104.
- Saher, R., Stephen, H., & Ahmad, S. (2021). Understanding the summertime warming in canyon and non-canyon surfaces. *Urban Climate*, 38, 100916. <https://doi.org/10.1016/j.uclim.2021.100916>
- Saher, R., Stephen, H., & Ahmad, S. (2020). Urban evapotranspiration of green spaces in arid regions through two established approaches: A review of key drivers, advancements, limitations, and potential opportunities. *Urban Water Journal*. <https://doi.org/10.1080/1573062X.2020.1857796>
- Roy, P., Pal, S. C., Chakraborty, R., Chowdhuri, I., Malik, S., & Das, B. (2020). Threats of climate and land use change on future flood susceptibility. *Journal of Cleaner Production*, 272, 122757.
- Schueler, T. (1987). Controlling urban runoff: A practical manual for planning and designing urban BMPs. metropolitan

- Washington Council of Governments. *Washington DC, USA.*
- Schueler, T. R., Fraley-McNeal, L., & Cappiella, K. (2009). Is impervious cover still important? Review of recent research. *Journal of Hydrologic Engineering*, 14(4), 309–315.
- Sesnie, S. E., Gessler, P. E., Finegan, B., & Thessler, S. (2008). Integrating Landsat TM and SRTM-DEM derived variables with decision trees for habitat classification and change detection in complex neotropical environments. *Remote Sensing of Environment*, 112(5), 2145–2159.
- Seto, K. C., & Reenberg, A. (Eds.). (2014). *Rethinking global land use in an urban era* (Vol. 14). MIT Press.
- Shaban, M. A., & Dikshit, O. (2001). Improvement of classification in urban areas by the use of textural features: The case study of Lucknow city, Uttar Pradesh. *International Journal of Remote Sensing*, 22(4), 565–593.
- Shah, B., & Ghauri, B. (2015). Mapping urban heat island effect in comparison with the land use, land cover of Lahore district. *Pakistan Journal of Meteorology* Vol, 11(22).
- Singh, A. (1989). Review article digital change detection techniques using remotely-sensed data. *International journal of remote sensing*, 10(6), 989–1003.
- Slonecker, E. T., Jennings, D. B., & Garofalo, D. (2001). Remote sensing of impervious surfaces: A review. *Remote Sensing Reviews*, 20(3), 227–255.
- Small, C., & Lu, J. W. (2006). Estimation and vicarious validation of urban vegetation abundance by spectral mixture analysis. *Remote Sensing of Environment*, 100(4), 441–456.
- SNAP Software, Help Document. (2019). Available online: <https://step.esa.int/main/toolboxes/snap> (accessed on 14 December 2020).
- Stefanski, J., Kuemmerle, T., Chaskovskyy, O., Griffiths, P., Havryluk, V., Knorn, J., & Waske, B. (2014). Mapping land management regimes in western Ukraine using optical and SAR data. *Remote Sensing*, 6(6), 5279–5305.
- Stow, D. A., DA, S., LR, T., & JE, E. (1980). Deriving land use/land cover change statistics from Landsat: a study of prime agricultural land. UNIV. CALIFORNIA, GEOGR. REMOTE SENSING UNIT/SANTA BARBARA CA/USA Source INTERNATIONAL SYMPOSIUM ON REMOTE SENSING OF ENVIRONMENT. 14/1980/SAN JOSE; USA; ANN ARBOR: ENVIRONMENTAL RESEARCH INSTITUTE OF MICHIGAN; DA. 1980; VOL. 2
- Subasinghe, S., Estoqe, R. C., & Murayama, Y. (2016). Spatiotemporal analysis of urban growth using GIS and remote sensing: A case study of the Colombo Metropolitan Area, Sri Lanka. *ISPRS International Journal of Geo-Information*, 5(11), 197.
- Sukawattanavijit, C., & Chen, J. (2015, July). Fusion of multi-frequency SAR data with THAICHOKE optical imagery for maize classification in Thailand. In *2015 IEEE International Geoscience and Remote Sensing Symposium (IGARSS)* (pp. 617–620). IEEE.
- Sweetman, C., & Ezpeleta, M. (2017). Introduction: Natural resource justice.
- Thakali, R., Kalra, A., Ahmad, S., & Qaiser, K. (2018) Management of an urban stormwater system using projected future scenarios of climate models: A watershed-based modeling approach. *Open Water Journal* 5 (2),1. <https://scholarsarchive.byu.edu/openwater/vol5/iss2/1>
- Thanh Noi, P., & Kappas, M. (2018). Comparison of random forest, k-nearest neighbor, and support vector machine classifiers for land cover classification using Sentinel-2 imagery. *Sensors*, 18(1), 18.
- Ullah, S., Tahir, A. A., Akbar, T. A., Hassan, Q. K., Dewan, A., Khan, A. J., & Khan, M. (2019). Remote sensing-based quantification of the relationships between land use land cover changes and surface temperature over the Lower Himalayan Region. *Sustainability*, 11(19), 5492.
- United Nations. (2008). United Nations expert group meeting on population distribution, urbanization, internal migration and development. United Nations Population Division. [http://sustainabledevelopment.un.org/content/documents/2529P01\\_UNPopDiv.pdf](http://sustainabledevelopment.un.org/content/documents/2529P01_UNPopDiv.pdf).
- United Nations. (2015). *Transforming our world: The 2030 agenda for sustainable development*. United Nations, Department of Economic and Social Affairs.
- UN World Urbanization Prospects. (2018). United Nations. <https://population.un.org/wup/>
- Venkatesan, A. K., Ahmad, S., Johnson, W., & Batista, J. R. (2011). System dynamics model to forecast salinity load to the Colorado River due to urbanization within the Las Vegas Valley. *Science of the Total Environment*, 409(13), 2616–2625.
- Waske, B., & Benediktsson, J. A. (2007). Fusion of support vector machines for classification of multisensor data. *IEEE Transactions on Geoscience and Remote Sensing*, 45(12), 3858–3866.
- Watson, S. J., Luck, G. W., Spooner, P. G., & Watson, D. M. (2014). Land-use change: Incorporating the frequency, sequence, time span, and magnitude of changes into ecological research. *Frontiers in Ecology and the Environment*, 12(4), 241–249.
- Wayback Machine. (2010). *Lahore\_Climate\_Data.txt*. <http://www.pakmet.com.pk/cdpc/Climate>
- Wu, Y., Li, S., & Yu, S. (2016). Monitoring urban expansion and its effects on land use and land cover changes in Guangzhou city. *China. Environmental Monitoring and Assessment*, 188(1), 54.
- Zia, S., & Shirazi, S. A. (2019). Spatio-temporal analysis of areas vulnerable to urban flooding: A case study of Lahore, Pakistan. *International Journal of Economic and Environmental Geology*, 10(3), 85–89.
- Zha, Y., Gao, J., & Ni, S. (2003). Use of normalized difference built-up index in automatically mapping urban areas from TM imagery. *International Journal of Remote Sensing*, 24(3), 583–594.
- Zhang, H., Li, J., Wang, T., Lin, H., Zheng, Z., Li, Y., & Lu, Y. (2018). A manifold learning approach to urban land cover classification with optical and radar data. *Landscape and Urban Planning*, 172, 11–24.
- Zhang, Q., Wang, J., Gong, P., & Shi, P. (2003). Study of urban spatial patterns from SPOT panchromatic imagery using textural analysis. *International Journal of Remote Sensing*, 24(21), 4137–4160.